Data Analysis of Carbon Corrosion in Polymer Electrolyte Membrane Fuel Cells

B. Westbroek

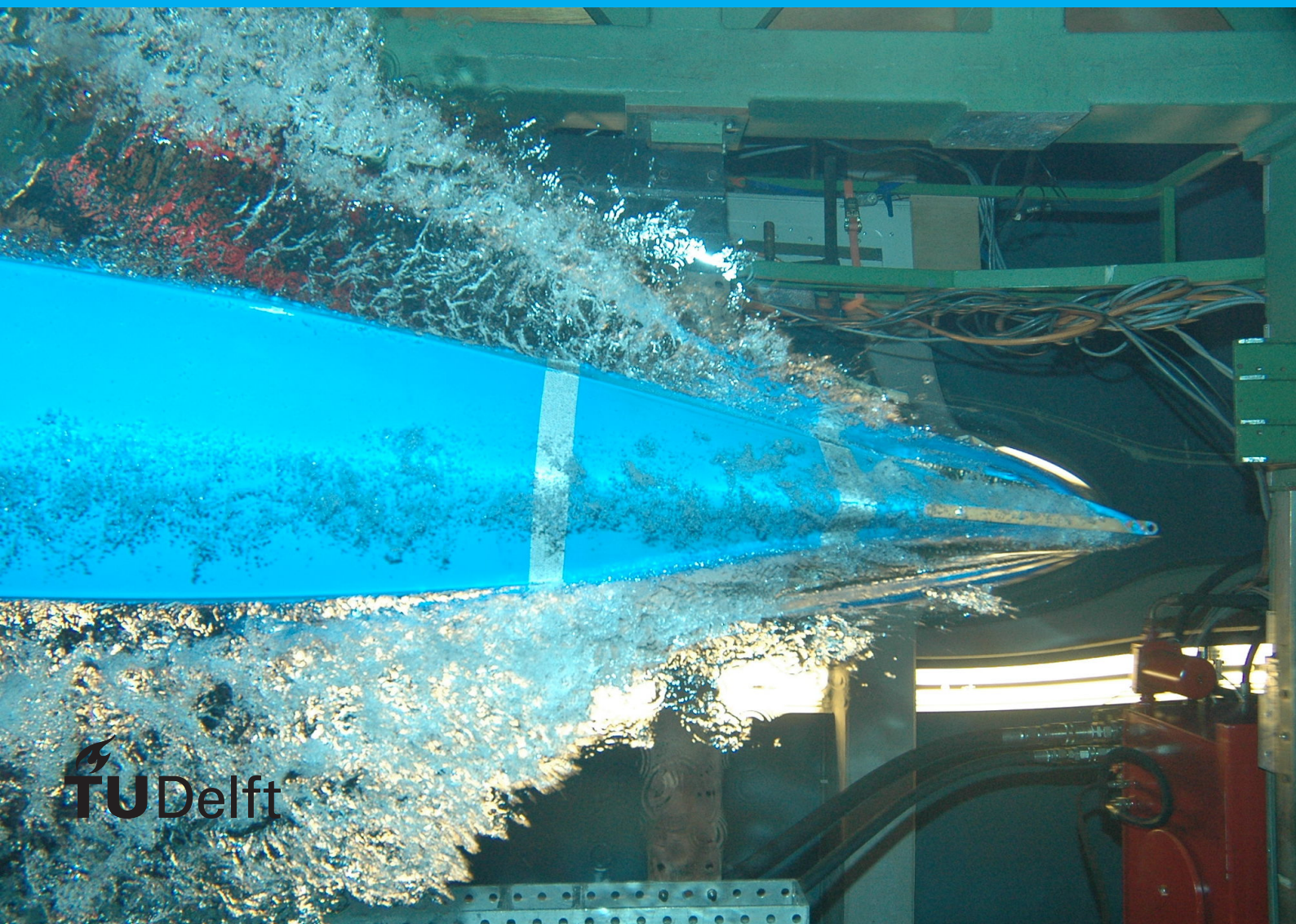

TU Delft

Data Analysis of Carbon Corrosion in Polymer Electrolyte Membrane Fuel Cells

by

B. Westbroek

to obtain the degree of Master of Science
at the Delft University of Technology,
to be defended publicly on Monday July 15, 2024 at 14:30.

Student number:	4388615	
Project duration:	July 1, 2023 – July 15, 2024	
Thesis committee:	Dr. ir. L. van Biert,	TU Delft, supervisor
	Dr. ir. H. Polinder,	TU Delft, chair
	Ir. A. Broer,	TU Delft, daily supervisor
	Ir. A. Rangel,	NEDSTACK
Rapport number:	2024.MME.8954	

An electronic version of this thesis is available at `http://repository.tudelft.nl/`.

TU Delft

Abstract

Carbon corrosion occurring on the cathode of a polymer electrolyte membrane fuel cell (PEMFC) leads to a reduction in the electrochemical surface area (ECSA). The ECSA is crucial for the efficiency and maximum power output of the fuel cell. Degradation of this component is detrimental to the overall performance of the system. Research into the mechanisms of ECSA degradation is essential for understanding and preventing fuel cell deterioration. The carbon in the electrode functions as a support material for the catalyst and provides the necessary electrical conductivity. Carbon corrosion can increase resistance between the electrode and the catalyst, and research suggests it may even cause the catalyst to detach from the electrode. This thesis investigates carbon dioxide emissions from a PEMFC during an accelerated stress test (AST), measured using a gas analyzer. The exhaust gases contain approximately 600 parts per million (ppm) of carbon dioxide, fluctuating by about 100 ppm throughout the day. A fluctuation of 80 ppm, attributed to changes in oxygen content during the operational and shutdown phases of the PEMFC stress cycle, was also identified. A formula was applied to remove these fluctuations to better understand the emissions. Carbon dioxide emissions were detected during the startup phase, when a hydrogen-air front is active at the anode, making carbon corrosion at the cathode likely. The area under the emission peak was determined and multiplied by the flow rate, providing an estimate of the carbon dioxide emissions and the corresponding carbon mass loss from the cathode. A secondary objective of this thesis was to validate a mathematical model of carbon corrosion with the obtained data. However, this was not possible with the current data set. The model does not account for the dynamic conditions of the stress test, which are typically significant contributors to carbon corrosion in a PEMFC.

Contents

Nomenclature/Acronyms

FC	fuel cell
FU	fuel utilization
PEMFC	proton exchange membrane fuel cell
H_2	hydrogen
CO	carbon monoxide
CO_2	carbon dioxide
GDL	gas diffusion layer
BPP	bipolar plate
MEA	membrane electrode assembly
H_2O	water or water vapor
LT	low temperature
RH	Relative Humidity
ppm	parts per million is a value for concentration
AST	Accelerated stress test
OCV	open circuit voltage
BoL	Beginning of Life
MoL	Middle of Life
EoL	End of Life

1

Introduction

1.1. Motivation for Advancing PEMFC Technology

Climate change is a pressing challenge for both current and future generations, extensively discussed in academic literature. Its impact has been observed globally across diverse regions [1]. To tackle this challenge, nations have committed resources to align with the objectives of the Paris Agreement, which aims to reduce greenhouse gas emissions [2].

To meet future energy demands while prioritizing environmental sustainability, there is a growing need to develop clean and renewable power sources. Clean energy refers to sources that do not emit harmful gases detrimental to human health and the global environment. Renewable energy, on the other hand, denotes resources that are either inexhaustible or rapidly replenished. Some examples of both clean and renewable sources are wind and solar energy [3]. The reliance on fossil fuels, which not only emit greenhouse gases but also deplete slowly over time, underscores their non-renewable and environmentally damaging nature. The shift away from polluting energy sources has sped up the advancement of solar and wind power technologies. This made them more competitively priced, and efficient [4].

Renewable power sources such as solar and wind energy induce fluctuation in the power grid due to the local weather conditions. These fluctuations can be filtered out using a buffer system [5]. Hydrogen can be considered for such a buffer system. A grid for future sustainability, free of polluting sources has been designed. The design uses wind and solar energy to provide the majority of the required power. Electrolyzers and fuel cells are used in a hydrogen-based buffer system. This buffer system reduces the fluctuations on the grid and produces enough power in low wind and solar conditions. In the paper by Samatli et al [6] more on this design can be found. A similar design is made for Australia in a paper by Boretti et al [7].

Another advantage of hydrogen as an energy carrier is the possibility to generate electric power close to end-users, which limits the power demand of the grid. Hydrogen transport via pipes instead of electric power via grid has been researched and shows promising results [8]. The integration of hydrogen into energy systems could address some of the difficulties of the energy transition by enhancing the resilience of power infrastructure [6].

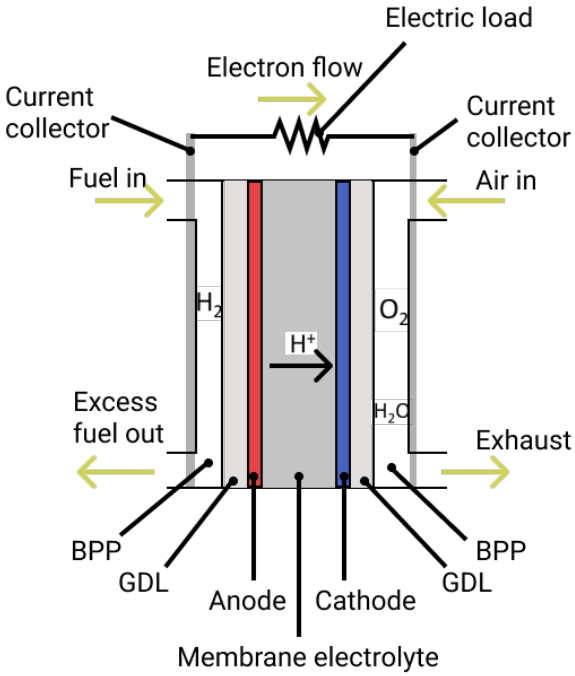

Figure 1.1: Schematic diagram of a PEMFC.

1.2. Fundamentals of PEMFC Operation

A polymer exchange membrane fuel cell (PEMFC), figure 1.1, comprises an anode and a cathode separated by a membrane. Humidified hydrogen gas (H_2) is introduced through a fuel intake into the cell, with the flow channels typically embedded in a bipolar plate (BP). These channels distribute hydrogen gas across the gas diffusion layer (GDL) surface evenly. The GDL fills with hydrogen, providing a consistent supply to the anode. At the anode, hydrogen undergoes oxidation. The resulting protons traverse the membrane, while electrons travel through the current collector to reach the cathode. At the cathode, oxygen (O_2) is reduced and reacts with hydrogen to form water (H_2O). Excess water is expelled through the exhaust. This reaction is exothermic, meaning that energy is released to the surrounding system, allowing power to be drawn from it.

To assess fuel cell performance, measurements of the electrochemical surface area (ECSA) are conducted. The ECSA is defined as the surface area of platinum catalyst that is electrochemically active. This is usually measured as the dispersion of platinum in m^2/g_{Pt} [9]. Various methods are commonly used for performance evaluation, for instance, cyclic voltammetry (CV) and electrochemical impedance spectroscopy (EIS). Performance degradation can occur due to a reduction in catalyst active surface area, an increase in electric resistivity and particle resistances or decrease in protonic conductivity, and pollution effects. Measurements on the ECSA often capture the cumulative effects of various damages, making it challenging to pinpoint the primary cause of performance loss.

This paper will focus on a specific type of damage known as carbon corrosion, which involves the gradual dissolution of the carbon-based electrode in the presence of air. This phenomenon primarily occurs at the cathode of the fuel cell and is heavily influenced by operating conditions.

1.3. Carbon corrosion at the cathode

Carbon corrosion is an oxidation reaction of carbon of the electrode with oxygen. Most electrodes of PEMFC are made from carbon-polymer composite. The carbon acts as support for the platinum and gives some structural strength to the electrode. Moreover, the carbon acts as an electron conductor,

the platinum at the cathode needs to receive electrons from the anode, the carbon chosen for this reason is a good conductor and has good stability in harsh environments [10]. Still, a slow decay of the carbon occurs under certain conditions. Elaboration on these conditions follows in section 2.2.

1.3.1. Challenges

A recurring challenge in various industries revolves around the question, 'How can we limit product degradation?' This pursuit extends to enhancing the longevity of diverse entities such as roads, buildings, engines, and now, fuel cells. Notably, the United States has set a target of achieving 8000 hours of fuel cell lifetime for light automotive applications [11]. Understanding the factors contributing to fuel cell degradation is paramount in achieving this goal. For instance, degradation of the carbon support at the cathode results in increased electron resistivity and can even lead to the deactivation of platinum catalysts [12]. Given that the cathode hosts the rate-determining reaction, any damage induced here can significantly reduce the fuel cells' performance [13].

1.3.2. Problem definition

In a preceding study, a model was developed to estimate the rate of carbon corrosion in the stack, utilizing parameters provided by Nedstack. However, this model remains unvalidated. For this thesis, I collaborated with Nedstack to investigate the rate of carbon corrosion in their PEMFC. To validate the model, we obtained data from an accelerated stress test (AST) conducted on a fuel cell.
Although, as will be explained in Chapter 3, the model has some reasons not to fit with data from an accelerated stress test due to the unknown severity of the dynamic behavior compared to the static behavior of the system. Despite this, an attempt is made to connect the data from the AST with the model. To facilitate this connection, it is necessary to gain insight into carbon corrosion at the cathode and start an analysis of the acquired AST data. Following the research question of this thesis: *How can we monitor carbon corrosion from PEMFC data gathered during a stress test, and what should change in order to use the data to validate the Nedstack model.*

Although, as will be explained in Chapter 3, the model has some reasons not to fit with data from an accelerated stress test due to the unknown severity of the dynamic behavior compared to the static behavior of the system. Despite this, an attempt is made to connect the data from the AST with the model.
The main question will be answered with the following sub-questions:

- When does carbon corrosion occur at the cathode of a fuel cell according to literature?
- How can we monitor carbon corrosion from AST data?
- What should change to either Nedstack's carbon corrosion model or the test setup in order to validate the model using AST data?

1.3.3. Report structure

Answering the research and sub-questions will be done in two stages. In chapter 2 an overview will be given on how a fuel cell operates. Literature about carbon corrosion at the cathode of a PEMFC will be compared in order to learn about corrosion rates and damages linked to corrosion of the electrode. Different parameters contributing to corrosion are written down because in order for it to be compared with a corrosion model. Chapter 3 is used to explain a mathematical model. A challenge is to validate this model for that knowledge about the functioning of this model is necessary. Chapters 4 and 5 will offer insight into Nedstack's AST, followed by an analysis of the data to examine the carbon corrosion rate during the test. The discussion shows how the data is handled. Undertaken steps are explained and an estimate for the corroded carbon is made from the data acquired. Chapter 5 also gives some recommendations for follow-up tests for the PEMFC and sensors that would be interesting to implement to the fuel cell and gas analyzer for the next setup design.

2

Background into PEMFCs

2.1. PEMFC at the beginning of life

In Figure 1.1, shows a schematic of a fuel cell, with the anode depicted in red and the cathode shown in blue. At the anode, hydrogen undergoes oxidation, while at the cathode, oxygen undergoes reduction. This electrochemical reaction is exothermic, meaning it releases heat. Both the anode and cathode are coated with a catalyst, typically the precious metal platinum, to lower the activation energy for the reaction. The half-reactions occur at the surface of this catalyst. During the anode half-reaction, hydrogen atoms are split into protons (H^+) and electrons (e^-). Protons, being acidic, migrate through the wetted membrane, while electrons, blocked by the semipermeable membrane, travel via an electron-conducting circuit to the cathode. At the cathode, oxygen molecules receive two additional electrons to form oxygen ions (O^{2-}). In the vicinity of the platinum catalyst, protons and oxygen ions combine to produce water (H_2O). The Hydrogen formation reaction from hydrogen and oxygen is given in formula 2.1. Reduction of catalytic activity, electron conductivity, and ion permeability can lead to increase in resistance, which is observable in IV-curves.

$$2\,H_2 + O_2 \longrightarrow 2\,H_2O \tag{2.1}$$

Figure 2.1 illustrates the polarization curve of a PEMFC, commonly referred to as the IV-curve. The graph plots cell voltage against current density. At zero current, the cell potential is at its peak, as depicted on the left side of the graph. This high voltage arises from the presence of oxygen at the cathode and hydrogen at the anode, creating a potential difference. However, an open electrical circuit prevents any current from flowing. Fuel crossover may slightly decrease the voltage, depending on factors such as membrane internal resistance and seal leakage. Moving slightly to the right on the graph, at 0.1 A/cm^2, a drop-off of approximately 0.15V is observed. This drop-off is attributed to activation losses, which occur when overcoming energy barriers at the electrode–electrolyte interfaces [14]. The catalyst used can significantly influence these losses. As the graph progresses to the right, a gradual decline in voltage is visible. Here, Ohmic losses supplement the activation losses. Ohmic losses vary with a factor proportional to the current density (U=R $\cdot$ I, where voltage equals resistance multiplied by current). Around 0.9 A/cm^2, mass transport losses begin to play a significant role, leading to a visible downward asymptote until it reaches its limit at approximately 1.2 A/cm^2. This example represents a model of a fuel cell in the initial stages of its lifespan. The values presented may vary depending on factors such as resistivity, operational temperature, pressures, partial pressures, and activation energy, which is dependent on catalyst availability.

In this next section the power-current curve and efficiency curve will be explained. The power current curve is the voltage produced at a certain current multiplied by that same current current via the formula P = I $\cdot$ U. In figure 2.2 two power to current density curves are given at two different manifold pressures. If the manifold pressure is increased a higher maximum power generated by the cell is possible. The

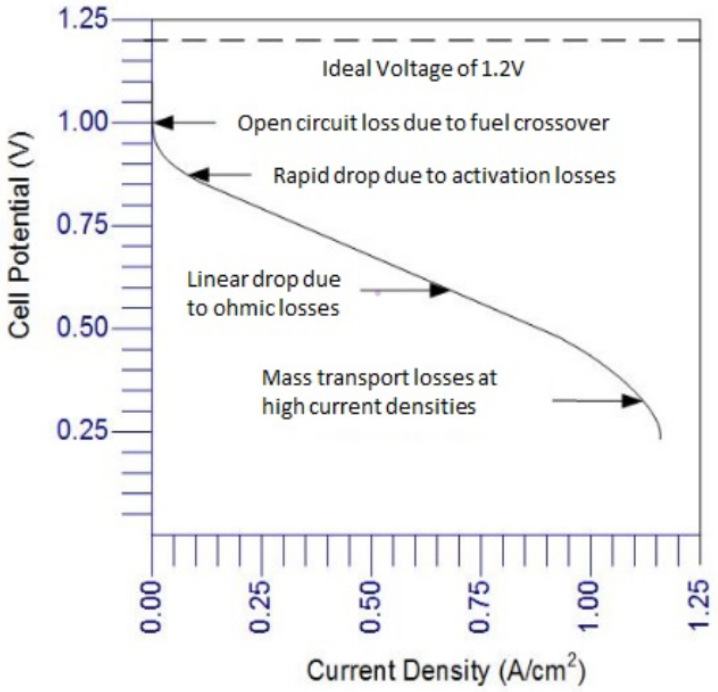

Figure 2.1: Polarisation curve of a polymer electrolyte membrane fuel cell [15]

difference between the two curves becomes more dominant when moving to higher currents. The higher pressures influence the mass transport limited region most.

2.2. Aging of PEMFC

A fuel cell experiences all sort of damage types as it gets used. These damages reduce the power output, reaction time, or efficiency. In Figure 2.3, both an IV-curve and a power curve depict the performance of an aging fuel cell. As the cell ages, the potential generated at a specific current density decreases, indicating degradation. Depending on the nature of the damage, the shape of the IV-curve may also change shape. The graph, sourced from Song et al. [17] shows accelerated degradation observed after 1400 cycles. The degradation evident in the IV-curve is also reflected in the power to current curve. No standardized criteria are set to define the end of life (EoL) of a PEMFC. In [18] a couple of research gaps are discussed concerning the EoL of PEMFCs. In that article, the author states that a set definition of EoL a PEMFC by the United States Department of Energy (USDoE) is not clearly defined. In chapter 5.4 IV-curves and Power curves (figure 5.5) are plotted. Note that they are similar in shape to Figure 2.3 the difference in power density comes from the difference in operation pressure during the measurement. Figure 2.2 shows what happens when the manifold pressure is increased.

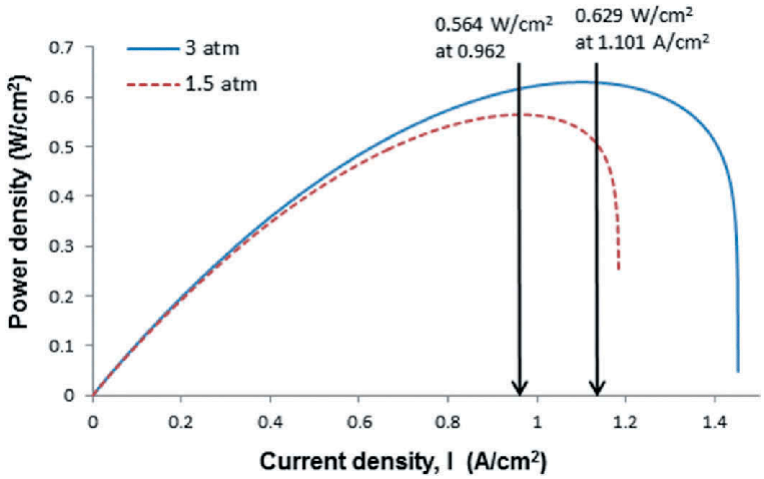

Figure 2.2: Power to current density curve of an PEMFC [16]. In this figure two different power curves are given for two different manifold pressures.

The change in output voltage, as observed in the IV-curve of a cell, can be attributed to variations in parasitic voltages. In equation 2.2, the cell potential (V) at a given current (i) is estimated. This voltage is determined by calculating the Nernst ideal potential, as shown in equation 2.3, and subsequently subtracting various parasitic voltages. These parasitic voltages fall into three main categories: activation potentials at the anode (2.4) and cathode (2.5), Ohmic resistance (2.6), and losses resulting from concentration reduction near the anode (2.7) and cathode (2.8)

$$V_{(i)} = E_{Nernst} - V_{AnodeAct} - V_{CathodeAct} - V_{Ohmic} - V_{ConcCathode} - V_{ConcAnode} \tag{2.2}$$

$$E_{Nernst} = E^0 + \alpha_1(T - T_0) + \frac{RT}{2F} \cdot ln(P_{H_2}\sqrt{P_{O_2}}) \tag{2.3}$$

$$V_{AnodeAct} = \frac{RT}{\alpha_a F} \cdot ln(\frac{i}{i_{0,a}}) \tag{2.4}$$

$$V_{CathodeAct} = \frac{RT}{\alpha_c F} \cdot ln(\frac{i}{i_{0,c}}) \tag{2.5}$$

$$V_{Ohmic} = i \cdot R_{Ohmic} = i(R_{electric} + R_{ionic}) \tag{2.6}$$

$$V_{ConcAnode} = \frac{RT}{nF} \cdot ln(\frac{i_{L,a}}{i_{L,a} - i}) \tag{2.7}$$

$$V_{ConcCathode} = \frac{RT}{nF} \cdot ln(\frac{i_{L,c}}{i_{L,c} - i}) \tag{2.8}$$

Nernst's equation (2.3) is a thermodynamically derived formula with empirically determined parameters. E^0 represents the ideal potential of the cell measured at 25° C (298.15 K) and 1 atm, typically found to be 1.229 V [19]. The parameter α_1 denotes the entropy change of the reaction and is approximately constant at -0.83 · 10^{-3} V/K. T is the temperature at which the fuel cell is operating and T_0 in Kelvin is the standard temperature of 298.15 K (again the 25° C at which α_1 is determined). R is the gas constant of 8.3143 J · mol^{-1} K^{-1}. F is the Faraday constant of 96487 C·mol^{-1} and in the natural logarithm the partial pressure of hydrogen P_{H_2}, and of oxygen P_{O_2}. This formula gives the base voltage. After this all the parasitic voltages are subtracted from the base voltage.

There are all sort of methods designed to asses the damage done to the fuel cell. Looking at the change of the IV-curve can already be useful in estimating the state of the fuel cell. It is important to note that not all damage is permanent, some damage done to the fuel cell can be reversed. This research rapport is about one specific type of damage which is not reversible, carbon corrosion at the cathode.

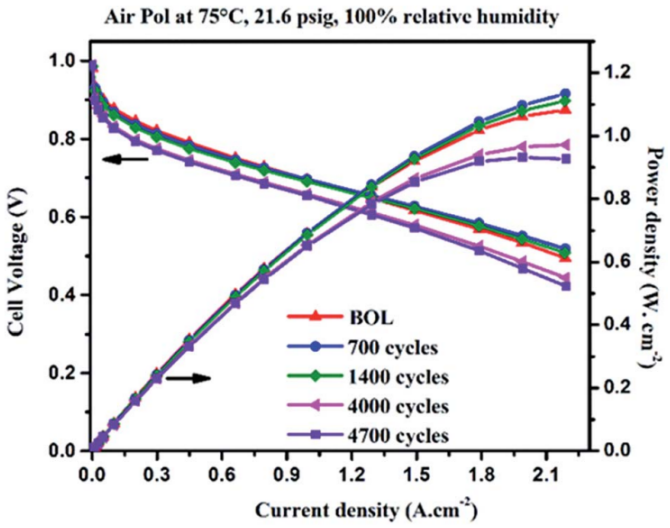

Figure 2.3: Polarisation, and power curve of an aging polymer electrolyte membrane fuel cell during and AST [17].

Carbon corrosion in a PEMFC is the degradation of the carbon-based electrode by a chemical reaction with oxygen to for carbon-oxides. This process occurs at the cathode and is influenced by different factors. The carbon dioxide or carbon monoxide formed leaves the fuel cell system via the exhaust. The carbon is permanently lost to the exhaust and makes the damage irreversible. To understand the damage mechanism of carbon corrosion is useful to look more closely at the surface of the cathode.

The triple-phase boundary, a crucial feature in proton exchange membrane fuel cells (PEMFCs), is situated on the surface of the electrodes. This boundary earns its name because it represents the interface where gas, solid, and liquid phases converge. In a typical PEMFC, the electrode comprises a carbon-polymer matrix that supports the platinum catalyst. Carbon serves a dual purpose, acting as an electron conductor and providing structural support for the platinum particles. These platinum particles are in direct contact with the reactant gas on one side and the membrane on the other. The membrane, essential for conducting protons, is kept wet to facilitate proton transport. Proton solve easily in water and act acidic H^+. At the cathode side of the electrode, oxygen gas and protons converge at the surface of the platinum particles to form water. The efficiency of this reaction is influenced by the structure and composition of the triple-phase boundary, making it a critical area for understanding and optimizing PEMFC performance. Deterioration of the carbon support can affect the conductance of electrons to the platinum and the bonding of the platinum within the cathode.

In figure 2.4a a schematic of a triple-phase-boundary of the cathode is shown. The gray areas are the carbon supports, the pink areas are the membrane, and the white areas are gas, containing oxygen. The green dot is a platinum particle. The electrons come from the carbon support. The oxygen is fed from the gas state. The protons come from the wetted electrolyte membrane in the form of acid diffusion driven by a concentration gradient, and by migration induced by an electric field resulting from a potential difference. In the figure some platinum particles are visible that do not touch all three different phases, these would not contribute to the cathode half-reaction.

Figure 2.4b shows 3 types of platinum agglomeration. From left to right through the figure are schematics of Oswald ripening, Platinum dissolution into the membrane, and Crystal migration. The catalyst is the reason the reaction works at a low temperature. Deactivation or clustering of the platinum particle leads to a reduced surface area for reaction. There are more types of platinum deactivation. Carbon corrosion leading to the detachment of platinum as discussed by Shao-Horn et al. can also lead to platinum deactivation, and reduce the electro-chemical surface area [21].

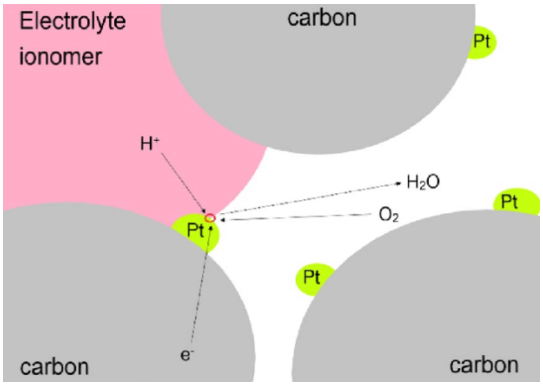

(a) shows a triple-phase-boundary at the cathode of a PEMFC. At these locations proton-ions, oxygen and the electrons come together to form water and finish reduction halve reaction [20].

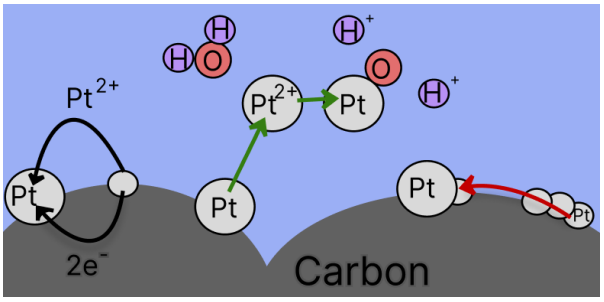

(b) shows 3 types of Platinum agglomeration. The black arrows show modified Oswald ripening, the green arrow shows platinum dissolution in the membrane and reacting with water, and the red arrow shows coalescence via Crystal migration. This figure is self-made but based on literature. The original figure can be found here [21].

Figure 2.4: a) shows a triple-phase-boundary at the cathode of a PEMFC. b) shows 3 types of Platinum agglomeration.

2.3. Carbon corrosion of the cathode

There are a couple of test methods to check for carbon corrosion. One of the methods is an in-situ test method where the exhaust gasses are analyzed for extra carbon monoxide and carbon dioxide emissions. If the electrodes would start to corrode and solve into gas, the gas would as via the exhaust into the ambient air. With a gas analyzer on the exhaust, the emissions can be checked for the occurrence of carbon corrosion. To check for when carbon corrosion takes place an accelerated stress test (AST) is developed to speed-up degradation of the fuel cell. In the AST different stages of the fuel cell are repeatedly induced. In literature is found when carbon corrosion is more likely to occur. In Zhao et al. the author states that during start-up and shutdown, high voltage operation carbon corrosion is occurring [22].

In certain instances within the fuel cell, various reactions can take place. One such reaction involves the formation of carbon monoxide from water and carbon, as shown in Formula 2.9b. Despite not being the preferred reaction due to its activation potential, it can still occur. Another reaction involves the formation of carbon dioxide, as depicted in Formula 2.9a. This reaction requires a lower potential, indicating its preference, as noted by Maass et al. [23]. In both reactions, water is a byproduct, and a threshold potential must be reached for the reactions to proceed. Given that this potential can typically be attained during normal fuel cell operation, which ranges from 0.6V to 0.8V per cell, these reactions are expected to occur, but at a very slow rate, as mentioned in 'Polymer Electrolyte Fuel Cell Durability' by Büchi et al. [24]

$$C + 2H_2O \longrightarrow CO_2 + 4H^+ + 4e^- \qquad E^0 = 0.207\ \text{V} \qquad \text{at } 25^\circ\text{C} \qquad (2.9a)$$

$$C + H_2O \longrightarrow CO + 2H^+ + 2e^- \qquad E^0 = 0.518\ \text{V} \qquad \text{at } 25^\circ\text{C} \qquad (2.9b)$$

$$CO + H_2O \longrightarrow CO_2 + 2H^+ + 2e^- \qquad E^0 = -0.103\ \text{V} \qquad \text{at } 25^\circ\text{C} \qquad (2.9c)$$

During startup carbon corrosion could occur. In this case not only at the cathode but also on the anode. If the fuel cell is not operating oxygen can leak from the cathode towards the anode, although this is unwanted. The oxygen present at the anode during startup can react with hydrogen from the anode or by drawing hydrogen ions from the cathode side. The preferred reaction for producing hydrogen ions at the cathode would likely be reaction 2.9a, as it has the lowest required potential. The mixing of oxygen and hydrogen at the anode can decrease the anode potential from 0V to -0.59V. Reiser et al. showed a reduction in the carbon layers after 5 hours of reverse current testing, resulting in a thinned cathode layer [25].

3

Model of PEMFC degradation

A model, for scientific purposes, is a simplified representation of system. A model is used to understand, explain or predict behaviour of that system. When designing a model the important features are described closely while other less important, or not important, features are neglected. For a PEMFC a carbon corrosion model, that describes the rate of corrosion at the cathode of a carbon-based electrode, is designed in [26].

3.1. Carbon corrosion model

The model uses 3 equations to find the carbon depletion of the cathode of a PEMFC, the Arrhenius equation. A kinetic governing equation and a rate equation are used to set up a material balance. In short, the model will be described for more information the original papers are recommended [26] [27]. Equation 3.1 is the Arrhenius equation. This equation is used to determine the amount of successful collision between particles. This is dependent of temperature and activation energy of the reaction.

$$k = Ae^{\frac{-E_a}{RT}} \tag{3.1}$$

A is the pre-exponential factor or frequency factor or pre-exponential rate and has unit the reciprocal of time (1/s). This factor says something about the frequency of collisions. Often determined empirically, it can also be calculated with the collision theory and transition state theory. E_a is the activation energy and is about 110.000 J mol^{-1}. R is the gas constant of 8.314 J mol^{-1} K^{-1}. T is the temperature in Kelvin. k is the rate constant in 1/s. For high temperatures (T) the fraction in the exponent of the Arrhenius equation converges to zero meaning that the exponent itself becomes 1, following k = A for large temperatures. For the PEMFC the rate constant in the Arrhenius equation is altered to fit more closely to the reaction at hand. $k_2(0)$ has as unit $mol \cdot m^{-2}s^{-1}$. It is still the rate constant but then the amount of particles reacting, and the area of reaction is also taken into account.

$$k_2 = k_2(0)e^{\frac{-E_a}{RT}} \tag{3.2}$$

The governing equation (eq.3.3) for r_2 gives the preferred, but rate-determining reaction for carbon corrosion. k_2 a parameter in the governing equation can be determined by the Arrhenius equation, (eq.3.2). $\Theta_{vac} \cdot \Theta_{COH}$ are two factors that give the fraction of vacant sites and the fraction of carbon oxides sides, with Θ_{COH} = 1 - Θ_{vac}. These surface oxides are experimentally determined to contribute to the rate equation. For this model, the vacant sites are set to 0.99995. p_0 and p_{0_ref} are used in a pressure ratio between the partial pressure for water vapor and reference pressure for water vapor respectively. In the exponent are α_{a2} is the anodic transfer coefficient for the carbon corrosion reaction. F is the Faraday constant. R is the gas constant. T is the temperature in Kelvin. V is potential of the fuel cell and $U2$ is the equilibrium potential for the reaction step.

$$r_2 = k_2 \cdot \Theta_{vac} \cdot \Theta_{COH} \cdot \frac{p_0}{p_{0\_ref}} \cdot e^{\frac{\alpha_{a2}F}{(RT))(V-U2)}} \tag{3.3}$$

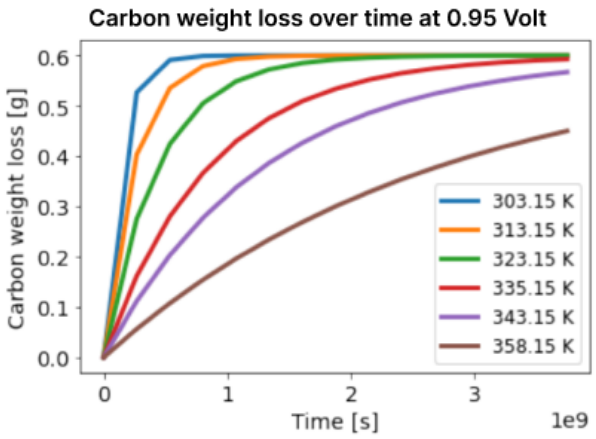

Figure 3.1: The carbon mass loss a 0.95V at different temperatures.

To track the carbon mass loss a material balance is set up. N_c is the carbon loading in the fuel cell and the derivative to time of the carbon loading gives the rate of change (eq.3.4). This rate equation is used by [26] together with the kinetic governing equation (eq.3.3) to find the carbon weight loss of the fuel cell. S_{BET} is the Brunauer-Emmett-Teller surface measurement. M_c is the molar mass of carbon.

$$\frac{dN_c}{dt} = -r_2 \cdot S_{BET} \cdot M_c \cdot C \tag{3.4}$$

The graph 3.1 from [27] show the mass of carbon lost over time. To find the carbon mass lost (eq.3.5) is used. This equation finds the carbon mass C from the carbon loading N_c, surface area A, and molar mass M_c. In 3.1 is visible that when the graphs level out at 0.6g, all the carbon in the fuel cell is lost. The model has had 6 different temperature settings in which the hottest fuel cell operation has the highest durability. A PEMFC usually runs at 335K or 62 degrees.

$$C = N_c \cdot M_c \cdot A \tag{3.5}$$

3.2. Improvements to the model

While going over the model a small mistake was noted in that the temperature changes in the model were only conducted for the change in r2, (see eq.3.3), and were not extended in the temperature dependency of the Arrhenius equation. This led to an unexpected carbon corrosion rate dependency on temperature. Figure 3.1 shows increased stability, and a slower corrosion rate, at higher temperatures. However, usually, reaction speeds increase at higher temperatures. After some searching, it was identified that the temperature dependency from the Arrhenius equations was not taken into account in the Python model. After modifying the model the carbon corrosion rate increases with the temperature. Figure 3.2 shows the modified model.

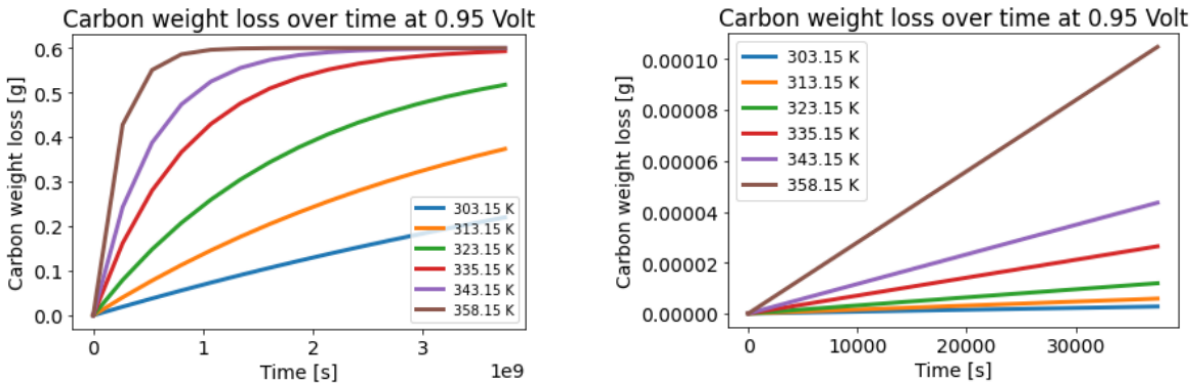

Figure 3.2: a) he carbon mass loss a 0.95V at different temperatures. The large difference are result in the changes in the Arrhenius equation. The rate equation for r2 (eq.3.3) is changed dependent by temperature twice, both in k_2 and the exponent. b) Shows the same model for a shorter time.

3.3. carbon corrosion at different potentials

The effect of a potential change on the corrosion rate is modeled and shown in figure 3.3. A large difference in corrosion rate is expected due to a change in potential. The temperature dependency of a the model is hard the validate from tests because fuel cell usually work at temperatures between 55°C and 65 °C. Higher temperatures can promote the oxygen reduction reaction but can also induce membrane drying. The graphs in figure 3.3 are made with the eq. 3.3 and eq. 3.4. In the kinetic governing equation the temperature was set to a constant 62 °C and V was made variable. The purple graph, potential of 1 Volt, shows an almost complete depletion of carbon material in the cathode after 1 billion seconds (31 years), while at 0.7 volts, the blue graph has no significant reduction in carbon by that time.

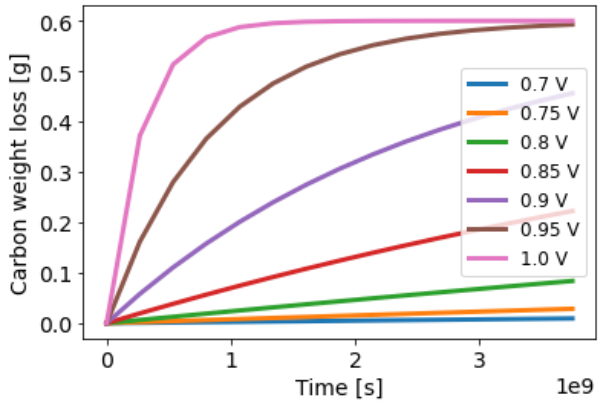

Figure 3.3: The carbon mass loss at 62 ° C at different cell potentials.

The tested fuel cell at Nedstack operated for a large part of the time at potentials of 0.6 Volt, which is not plotted in this figure but would give an even lower carbon corrosion rate according to the equations given in section 3.1. If the model is true the carbon dioxide emission from carbon corrosion are to small to be measured by the gas analyzer used. This will be further explained in chapter 5.

4

Accelerated stress test

An accelerated stress test (AST) is designed to uncover degradation mechanisms and test for design errors in systems. Usually, a certain product can last a long time in average conditions, but during an AST rough conditions are applied to induce wear and damage to the system in evaluation at a faster rate. In the case of a PEMFC, a fuel cell could last a long time. Systems lasting 20.000 hours are already operational [28]. Designing a test that lasts for these stretches of time is not convenient, so an AST is used to learn about the degradation mechanisms of the designed system at a faster rate.

4.1. AST at Nedstack

Nedstack has its own test facilities. In the lab they have a short stack fuel cell connected to a series of sensors. These sensors continuously record data, storing it for future analysis. The fuel cell's exhaust gases are directed to a gas analyzer, which measures the quantities of various gases in the mix. Positioned between the gas analyzer and the fuel cell is a chiller, which serves to lower the temperature of the exhaust gases to a constant 3°C. Figure 4.1 shows a schematic of the setup. The chiller reduces water vapor content in the air. The condensed water is removed before the analyzer. This process not only reduces the water vapor fraction but also maintains it at a near-constant level. Equation 4.1 shows an estimation for the amount, in parts per million, of water vapor in the air at 3°C based on the universal gas law. 101,325 Pa is the standard pressure of the atmosphere. 758 Pa is the vapor pressure of water at 3°C

$$H_2O[ppm] = \frac{758[Pa]}{101,325[Pa]} \cdot 1,000,000 = 7481ppm \tag{4.1}$$

The sensors on the fuel cell collect data at one-second intervals, which is then stored on a server. The data includes timestamps, load settings in Ampere, load in mA/cm², stack voltage, cathode airflow, anode air purge flow, anode nitrogen purge flow, hydrogen flow through the anode, temperature measurements of the intake and exhaust of the stack, as well as from the cathode and anode individually. Additionally, relative humidity measurements are taken at both the anode and the cathode. The PEMFC short stack comprises 5 cells in series, each equipped with its own voltage sensors. Intake and exhaust pressures of the anode and the cathode are also recorded.

The gas analyzer measures and stores data with a 1-second interval as well. The timestamp of the gas analyzer, although correct, does not match the state of the fuel cell at the same timestamp. This is due to the physical distance between the fuel cell and the gas analyzer. Any distance would have induced a time delay between the matching measurements a cycle of the fuel cell operation. The measurements recorded by the gas analyzer include flow rates in normal liters per minute, concentrations in percentage or parts per million, and pressures in pascals. Specifically, it measures the concentrations of carbon monoxide, carbon dioxide, hydrogen, and oxygen. The concentration of carbon monoxide and carbon dioxide are very interesting to observe. A change in concentration following from carbon corrosion occurring at the cathode may be observed. In chapter 5 the concentration change will be

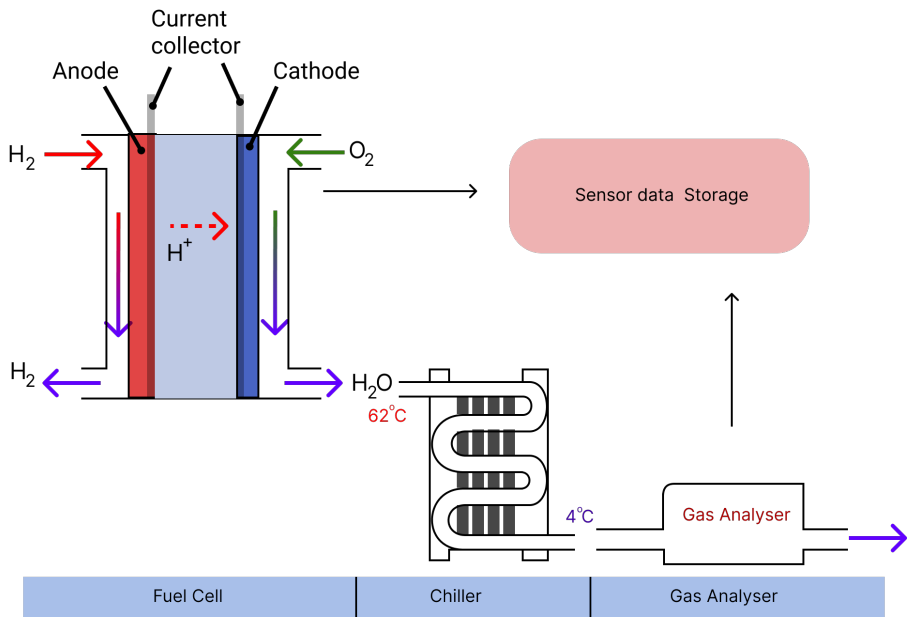

Figure 4.1: A Schematic of the test setup. The fuel cell exhaust is connected to a chiller. From the chiller, the gases flow into the gas analyzer.

explained further.

4.2. Data visualization

In this section some visualizations of the data are made. Figure 4.2 shows the measurement of carbon dioxide over the full duration of the test. The test took 580000 seconds, which is about a week. During that time the fuel cell has done 1300 cycles each taking 7 minutes and 24 seconds. In this figure a seemingly thick blue line is plotted with 7 local maxima and minima. These fluctuations are due to the night-day cycle, which has different carbon dioxide concentrations. These fluctuation in the ambient conditions are also measured by the gas analyser.

In figure 4.3 a visualization is made of the AST. The fuel cell operation is a current-driven process. The demand on the current changes the potential. The cycle begins with a steady-state operation of the fuel cell lasting 285 seconds, followed by a shutdown phase where the load is switched off, transitioning the fuel cell to open circuit voltage (OCV). During shutdown, the anode undergoes a 55-second nitrogen gas purge to minimize damage. Subsequently, an air purge of the anode is conducted over approximately 56 seconds. The fuel cell then enters the startup phase, initiating hydrogen flow through the anode. The voltage rises rapidly as the current demand is steadily ramped up over 45 seconds, reaching 150 Amperes. Figure 4.3b displays a voltage plot of the AST cycle, taken from a cycle in the middle of the test, with a plot duration of 10 minutes (600 seconds). Throughout this chapter, this span of 10 minutes of the cycle within the test is revisited to make comparing phases during the cycle easier. The red bar in the figure 4.3 indicates the shutdown phase of the fuel cell.

Figure 4.3b shows the fuel cell potential. On the left side of the graph, at time is 0, and the fuel cell operates at steady state at about 0.6 A/cm^2. Moving to the left in the graph, at 210 seconds, the fuel cell goes into OCV, seen as a spike in voltage to 1.0 Volt. The voltage produced starts to drop when the purging with nitrogen gas starts at the anode. When the reactant gasses are fed back into the fuel cell the potential starts to rise rapidly to 1.0 Volt. When the load is applied, and a current is drawn, the potential drops to 0.6 Volt. Figure 4.3c shows the airflow through the cathode. The flow is set to 25 normal liters per minute except for a sort period during the shutdown phase. The reason for this, as explained by Nedstack, is that during this period nitrogen is purged at the cathode. No record of that is found in the data set.

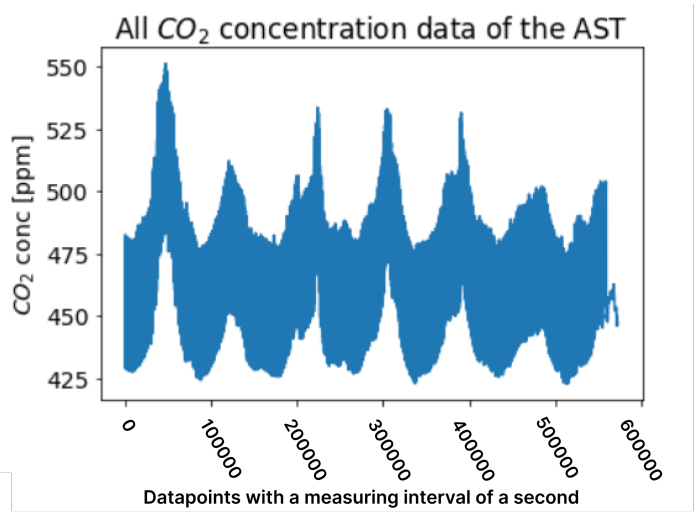

Figure 4.2: Concentration data of CO_2 of the whole AST. In this figure the individual cycles are not recognizable, but what is visible is 7 local minima and maxima which are the day and night cycle occurring over the duration of the test.

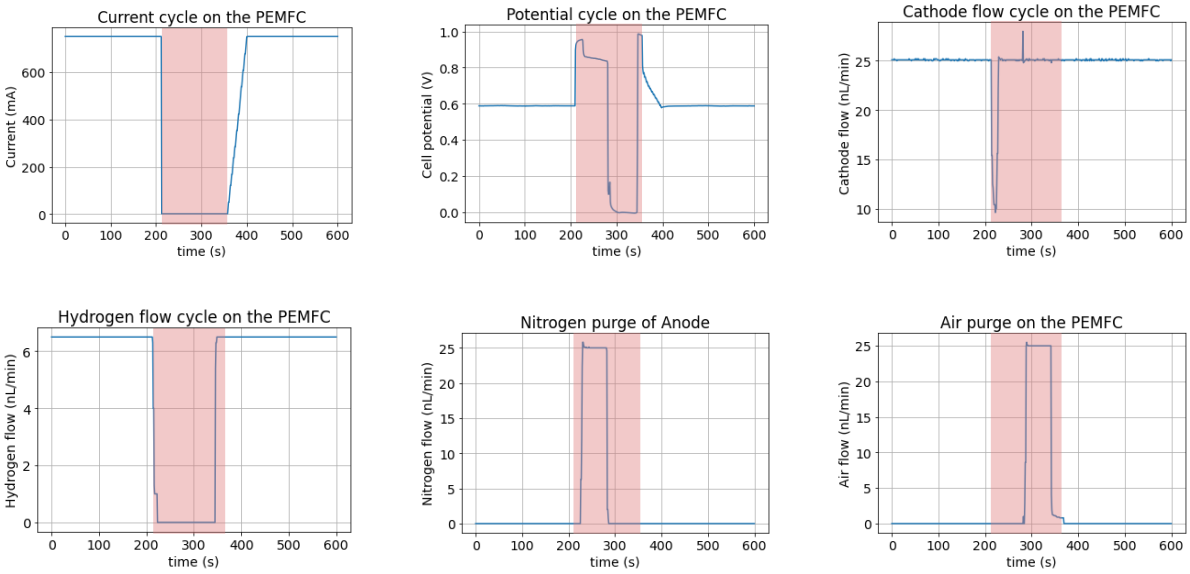

Figure 4.3: (a) Current demand of the fuel cell stack. (b) Potential during current demand change. (c) Flow through the cathode (d) Hydrogen flow through the anode. (e) Nitrogen purge through the anode. (f) Airflow through the anode before startup.

Figure 4.4 shows carbon dioxide measurement data of the gas analyser. From left to right in the graph, the carbon dioxide starts high at 512 parts per million, during steady-state operation, and decreases to 460 ppm during the shutdown phase of the fuel cell. The carbon dioxide value stays nearly the same until the startup of the fuel cell then a small peak is observed after which the carbon dioxide value increases to 513 ppm. The change of 52 ppm is about 10% of the carbon dioxide fraction. In chapter 5 this change will be explained further.

In Figure 4.4, a measurement of carbon monoxide during one cycle of the AST is depicted. The carbon monoxide sensor exhibits a small calibration fault, apparent as negative values for CO in the graph. From left to right, the values hover slightly negative around -0.2 ppm. This level is maintained throughout the graph exempt for a peak reaching 0.15 ppm. Interestingly, this peak coincides with the peak observed in the carbon dioxide measurement. This observation will be further discussed in section 5.2.1.

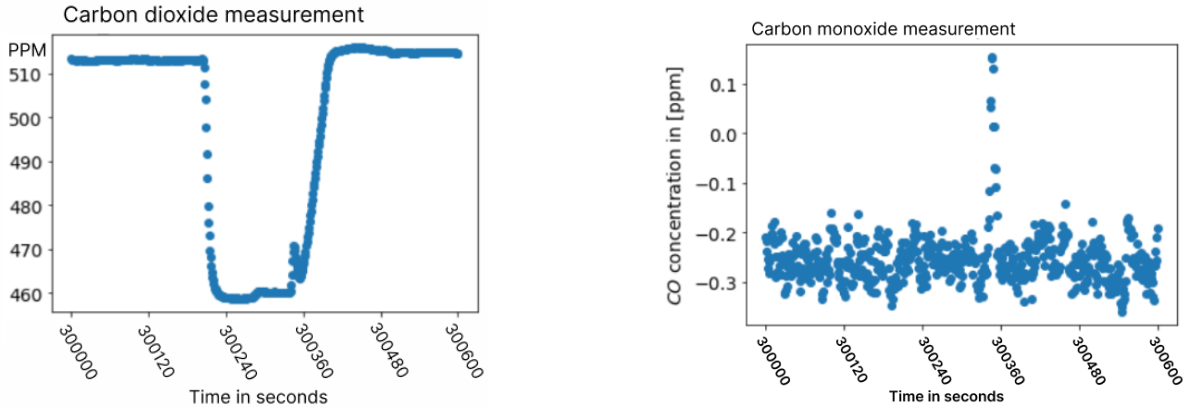

Figure 4.4: a) Shows the carbon dioxide measurements from Nedstack's gas analyzer on a PEMFC short stack. This is a little over one cycle in duration from data about halfway through the AST. b) Shows the carbon monoxide measurement of the same duration. The negative values of the carbon monoxide measurement is a calibration fault.

Figure 4.5a displays the oxygen measurement from the gas analyzer. During operation, the oxygen content in the fuel cell exhaust decreases to 12%, as shown in the first 200 seconds in the graph. Moving to the right, a peak with a maximum of 21.5% oxygen is observed during fuel cell shutdown. Upon startup of the fuel cell, the oxygen content in the cathode exhaust, as measured by the gas analyzer, decreases back to 12%.

Hydrogen content in the exhaust gas is monitored, and the measurements of one cycle are plotted in figure 4.5b. During operation, the hydrogen percentage in the exhaust is 0.28%, increasing to 0.49% during shutdown, as seen by the peak in the middle of the graph. During startup, the hydrogen percentage in the exhaust returns to 0.28%.

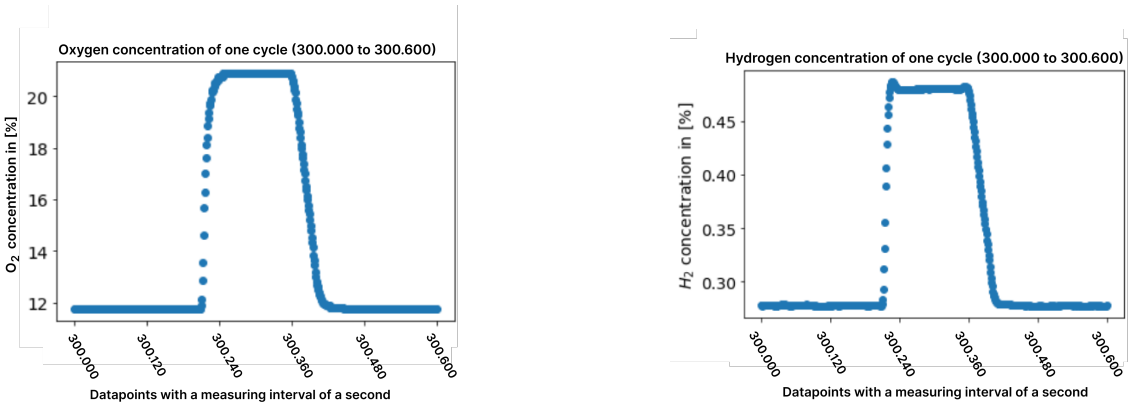

Figure 4.5: a) Shows the oxygen measurements from Nedstack's gas analyzer on a PEMFC short stack. This is a little over one cycle in duration from data about halfway through the AST. b) Shows the Hydrogen measurements from Nedstack's gas analyzer on a PEMFC sort stack.

In this chapter a large part of the data is presented. Notable are the large fluctuations in the carbon dioxide data during the day visible in figure 4.2. A potential sensor that never exceeds 1.0 Volt in figure 4.3B. A reduction in flow through the cathode in figure 4.3C. Large changes in the carbon dioxide fraction within one cycle (figure 4.4A) and negative values for the carbon monoxide fraction (figure 4.4B). These figures will be discussed further in chapter 5.

5

Data analysis

5.1. Compensating time delay

The datasets from the fuel cell and the gas analyzer exhibit a time offset in recording certain events. For instance, during fuel cell shutdown, the load disconnection stops the electron current. Subsequently, the fuel cell enters open-circuit voltage (OCV) mode, and after a couple of seconds, nitrogen purging starts. These events manifest as a voltage spike, succeeded by a gradual voltage decline until reaching 0 volts. The gases discharged from the fuel cell are directed to the gas analyzer via a chiller. However, the spatial separation between the fuel cell and the gas analyzer, combined with finite propagation speeds in the pipes, introduces a time lag between the gas measurements and the corresponding events at the fuel cell. Aligning the datasets was an initial step in the analysis process. In Figure 5.1, the occurrences in the gas analyzer are synchronized with those in the fuel cell. The upper graph displays the cell potential directly from the PEMFC and the oxygen concentration data form the gas analyzer. To facilitate comparison, several colored lines are added to highlight corresponding events.

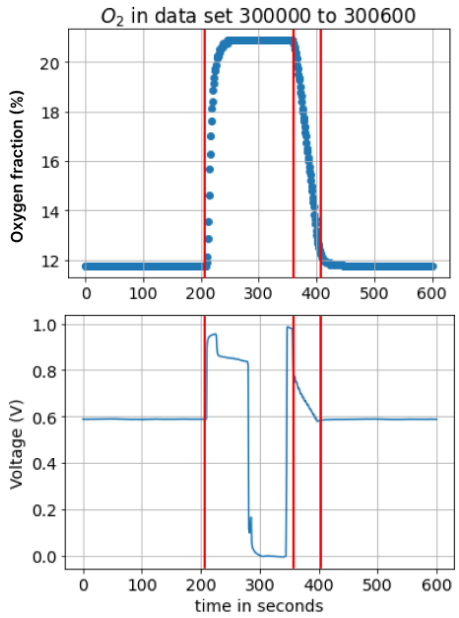

Figure 5.1: Alignment of the oxygen data from the gas analyzer with the potential of the fuel cell data.

5.2. Evaluation of the carbon dioxide data

5.2.1. Oxygen fraction compensation

Carbon dioxide and carbon monoxide can both form during carbon corrosion [29]. The preferred reaction is the production of carbon dioxide, although carbon monoxide can still be generated under certain conditions, such as high temperature or insufficient oxygen. In the data presented in Figure 4.4, the carbon dioxide concentration fluctuates between 460 and 512 ppm during operation, with a noticeable peak around the 400th second. These fluctuations can be partly attributed to variations in oxygen content during the stress cycle, as shown in Figure 4.5. The significant change in oxygen concentration, from 21.5% to 12%, represents nearly one-tenth of the gas mixture, increasing the carbon dioxide concentration by around 60 ppm. Additionally, water vapor formed during the reactions exists partially as liquid and partially as vapor in the exhaust gases. However, before reaching the gas analyzer, the air is cooled to a steady 4 degrees Celsius by a chiller. This cooling process causes water vapor to condense and be drained, reducing the number of particles reaching the gas analyzer. This also changes the flow rate through the gas analyzer slightly. To account for variations in oxygen content, Equation 5.1 is implemented for CO_2 compensation. A relative compensation method was chosen instead of a mass balance method because not all mass fractions are known. The cathode intake gas composition fraction is not measured. The water volume removed by the chiller and the water vapor fraction in the mixture can only be estimated.

$$CO_{2\_Compensated} = CO_{2\_Measured} \cdot \frac{100}{100 - O_{2\_Measured}} \tag{5.1}$$

This equation effectively removes all the oxygen from the mixture, resulting in a more consistent carbon dioxide fraction. By applying this formula, the overall CO_2 fraction in the air appears larger. In the equation $O_{2\_Measured}$ is the oxygen fraction measured by the gas analyzer as a percentage. $CO_{2\_Measured}$ is the measured fraction of carbon dioxide in parts per million, and $CO_{2\_Compensated}$ is the compensated carbon dioxide fraction in parts per million. The resulting plot is shown in figure 5.2. The horizontal axis represents time, while the vertical axis displays the parts per million of carbon dioxide in the mixture. The red lines mark the beginning of characteristic points in the curve, often coinciding with events of power changes.

Figure 5.2 B) illustrates a nearly constant carbon dioxide content, with the exception of a small peak. This peak coincides with the startup of the fuel cell, during which hydrogen is introduced into the anode chamber while air containing oxygen is present. This sets the stage for a reaction between oxygen and hydrogen on one side of the membrane, while hydrogen ions migrate from the cathode to the anode via the membrane. Meanwhile, water on the cathode side can be broken down into hydrogen and oxygen. The hydrogen then migrates into the membrane. Oxygen, on the other hand, reacts with carbon at the cathode, forming carbon oxides, predominantly carbon dioxide, and possibly carbon monoxide. The potential of the anode can decrease during the hydrogen-air front with -0.59 Volt. The potential difference between the anode and the cathode will rise, potentially high enough for electrolysis of water to occur, to ca. 1.3 Volt [22]. Carbon corrosion during startup is considered highly detrimental [30]. Besides the time delay between the fuel cell and the gas analyzer, a time delay between instruments within the gas analyzer might be possible. Although, the internal geometry of the gas analyzer is unknown to me. A sensitivity analysis is conducted in case a small time delay between the oxygen measurement and carbon dioxide measurement exists.

The spike in CO is an indication that the potential between the anode and the cathode is 1.2 Volt or higher [31]. The small carbon monoxide production can be seen in figure 4.4b. Although the measured voltage at that time is 1 Volt, the CO-formation indicates a higher potential of about 1.2 Volt. The carbon corrosion rate, as described in [25], increases rapidly between 1.2 and 1.3V. In other papers is found that carbon monoxide formation could also occur at lower potential. So why it is much more visible at higher potentials could be caused by that the formation reaction of CO increases at higher potentials and was at lower potentials not so pronounced or a further evolution reaction of CO to CO_2 (eq.2.9c), occurs that could deplete the carbon monoxide.

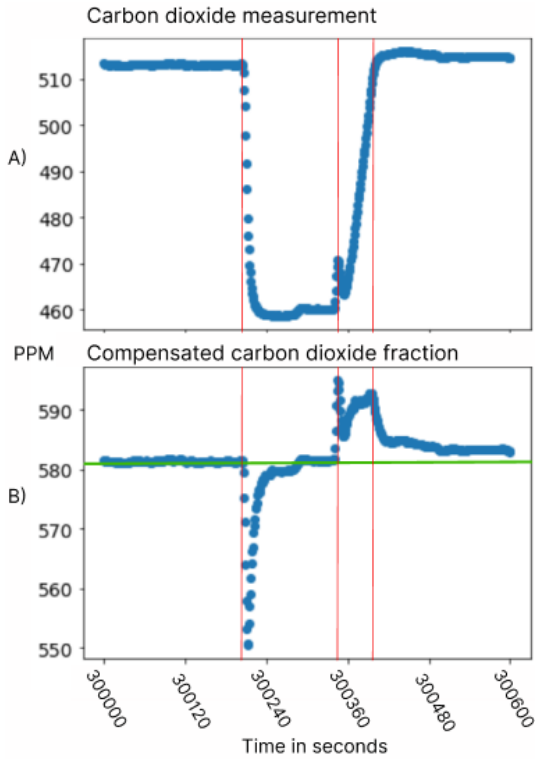

Figure 5.2: Carbon dioxide data from the gas analyzer. Figure 5.2a represents the unprocessed data, the same graph as shown in figure 4.4a. Figure 5.2b shows the oxygen content compensated data. The green line show the base value of carbon dioxide in air

5.2.2. Gas flow compensation

The gas flow through the gas analyzer is found to be fluctuating. In figure 5.3 the flow through the gas analyzer is shown for one cycle of the AST. The scatter on the measurement is significant, still, a trend in the scatter is visible. Figure 5.3b shows the trend of the flow through the gas analyzer. The filter uses the 10 nearest points to find the value. This method underestimates maxima and minima but is fairly accurate still. The filtered trend looks quite constant for the most part. Two characteristic points are still notable. One is a peak and the other a valley. These maxima and minima respectively are occurring during shutdown and startup of the fuel cell. In order to estimate the accumulative sum of extra carbon dioxide emitted, this is the carbon dioxide produced from carbon corrosion. The gas flow speed will be an important factor for the calculation. An estimation for the amount of corroded carbon will be made in section 5.3. First, the amount of carbon dioxide per volume passing through the gas analyzer instead of carbon dioxide in the gas analyzer per unit time needs to be found. For that the flow through the gas analyzer is used to find the carbon dioxide fraction passing through the gas analyzer per volume, instead of the fraction of carbon dioxide per time. The fluctuations in the flow speed give a slanted view of the corrosion speed. An extreme example would be if the fuel cell is not operating and the flow in the gas analyzer is zero no carbon corrosion would be occurring, although the measured carbon dioxide in the gas analyzer could be above the ambient carbon dioxide in the air. This would suggest continued carbon corrosion although this is not the case.

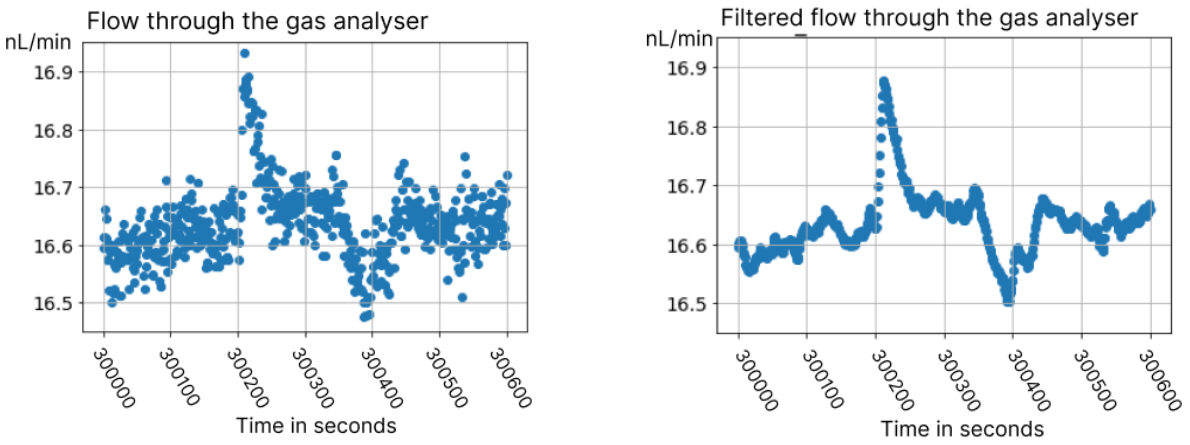

Figure 5.3: a) Gas flow through the gas analyser during a cycle of the AST. A certain trend in the figure is visible. b) The flow though the gas analyser with an applied filter to remove the scatter of the flow as seen in figure 5.3a

5.3. Estimation total corroded carbon

An estimation of the total corroded carbon is made. For this, an approximation for the base value of carbon in the air is made for the cycles under review. The base value in the air changes a lot, as stated in 5.2.1. The difference between every measurement and the estimated base is determined. That gives the extra concentration of carbon dioxide in the mix. The extra CO_2, assumed to be the effect of carbon corrosion. The concentration increase multiplied by the flow rate gives a concentration in a volume per time. The volume for a mol gas can be calculated with eq.5.3. This equation is derived from eq.5.2 and gives a relationship between the pressure P, the Volume V, the universal gas constant R, the temperature T, and the number of moles of gas. The pressure is measured and is approximated the standard pressure in Pascal. The temperature is 4 Kelvin and R is constant 8.314 J $\cdot$ mol^{-1} $\cdot$ K^{-1}. n can be set to 1. Using the measurements from gas analyzer 22.413 L $\cdot$ mol^{-1} is found for the molar volume.

$$P \cdot V = n \cdot R \cdot T \tag{5.2}$$

$$\frac{V}{n} = \frac{R \cdot T}{P} \tag{5.3}$$

The flow through the gas analyzer is measured with the same measured with an interval of one measurement every second. The flow is about 17 liter per second but a more accurate depiction of the flow can be seen in figure 5.3b. The fraction of carbon dioxide multiplied with the flow through the gas analyzer per time step divided by the molar volume gives the mol carbon lost per second. For that, it is necessary to recall that 1 mol of carbon lost from the cathode is equal to one mol of extra CO_2 measured. That 1 to 1 fraction is visible in the chemical equation 2.9a. Equation 5.4 gives the formula that calculated the carbon lost from the cathode, based on the extra CO_2 emissions.

Figure 5.4a shows a schematic of how the area under the peak is determined in a calculation. The green line is the estimated ambient CO_2 fraction in the air. The red area in the graph is the extra CO_2 emitted. Figure 5.4b shows a possible explanation for the peak downwards in figure 5.4a. During the minima, possible nitrogen purging occurs at the cathode, according to Nedstack, although no data was stored on this event. While an allocation for the possibility of purging at the cathode was made in the data frame. If pure nitrogen is purged at the cathode all other fraction of gas would get reduced. This seems the case in the compensated carbon dioxide data, but not clear in the other gases measured by the gas analyzer. The data collected during the nitrogen purging is not taken into account for the estimation of the carbon lost. Although, carbon corrosion could occur during the OCV phase occurring during purging.

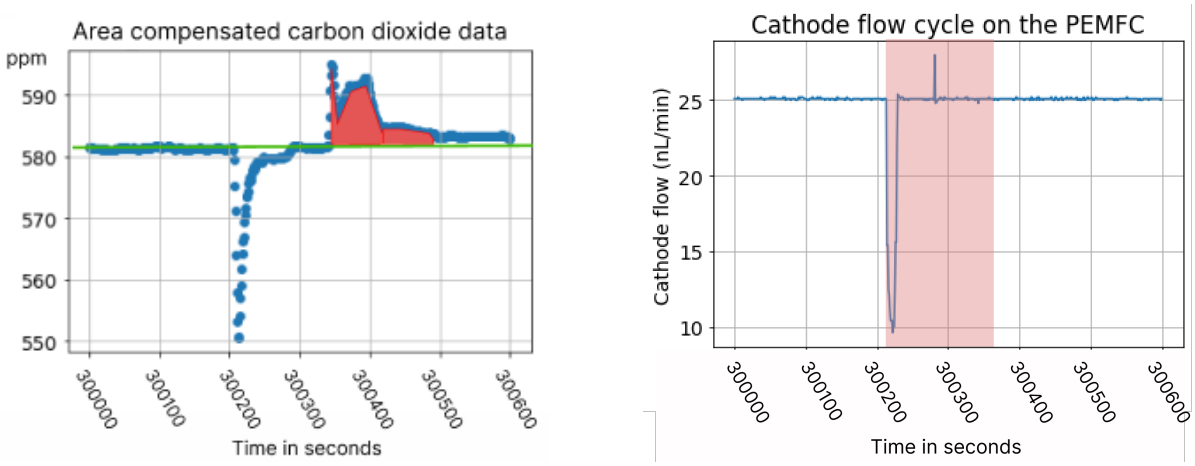

Figure 5.4: a) From the same data in figure 5.2B and formula 5.1 This graph is made the green line indicated the ambient carbon dioxide in the air. The red area indicates the extra CO_2 in the gas analyser. b) shows the a stagnated flow through the cathode at which nitrogen purging through the cathode takes place according Nedstack

The parameters of equation 5.4 are explained in the flowing text. G is the amount of carbon lost in mol per second. C_{meas} is the CO_2 concentration measured in the gas analyzer. C_{amb} is the ambient CO_2 concentration in the air. Q is the flow rate in normal liters per minute, measured every second. V_m is the volume of 1 mol at 4 degrees Celsius, following from (eq. 5.3). s is a factor of 60 to convert from minutes to seconds. Finally, P is a constant to convert from parts per million to a fraction between 0 and 1.

$$G = \frac{(C_{\text{meas}} - C_{\text{amb}}) \cdot Q}{V_m \cdot s \cdot P} \tag{5.4}$$

$$G = \frac{(590.943ppm - 581.5ppm) \cdot 16.5643\frac{L}{min}}{22.413\frac{L}{mol} \cdot 60\frac{sec}{min} \cdot 1,000,0000ppm} = 1.163852e-7\frac{mol}{sec} \tag{5.5}$$

To find the sum of extra carbon dioxide emission over a length of time, this formula can be recalculated for every time step. The sum of all the extra CO_2 emissions over the length of a cycle for example will give the carbon lost per cycle. For the cycle displayed in figure 5.4 the carbon mass lost is estimated to be 7.22e-06 mol. If this peak is similar in size over the whole AST and it is in fact carbon corrosion, then over the length of the AST, 0.130 gram of carbon is lost to CO_2.

0.130 gram of carbon lost is not large enough to expect a significant demising carbon corrosion rate due to loss of carbon at the cathode, according to the carbon corrosion model by Nedstack. To follow up on that thought cycles early, mid, and late in the AST are compared. Table 5.1 shows the amount of extra carbon dioxide passed through the gas analyzer during the carbon dioxide peak during startup. The values in the table are not that different in size. Measurement 300000 sticks out.

5.4. Reduction of performance of the fuel cell

From the data, two curves are made to visualize performance degradation. Figure 5.5a shows the change of the polarization curve during the test. In the Begin of life (BoL) is indicated with a blue color, mid of life (MoL) with orange, and End of Life (EoL) with green. A red arrow is placed in the figure to show the aging of the fuel cell. Degradation is recognizable by the reduced potential given at a current. This follows from an increased resistances and activation losses. When looking at the polarization curve, the activation losses can be recognized at left side of the graphs. Early in the stress test this drop is 0.2 volt, from 1.0 to 0.8. At the end of the test the drop is about 0.23 Volt, from 1.0 to 0.77 Volt. The increased resistance is visible as the increased slope, between 0 and 700 mA, when the fuel cell ages. Although the change in polarization curve does not indicate carbon corrosion specifically it does show a reduction in fuel cell performance.

Time into test [sec]	CO_2 [Mol/peak]	Description
100000	6.48e-06	early in AST
150000	6.55e-06	
200000	6.58e-06	
250000	6.19e-06	
300000	7.22e-06	mid in AST
350000	6.04e-06	
400000	6.17e-06	
450000	5.95e-06	
500000	6.11e-06	late in AST

Table 5.1: Estimated carbon lost per peak. The length of the peak is taken to be 70 data point

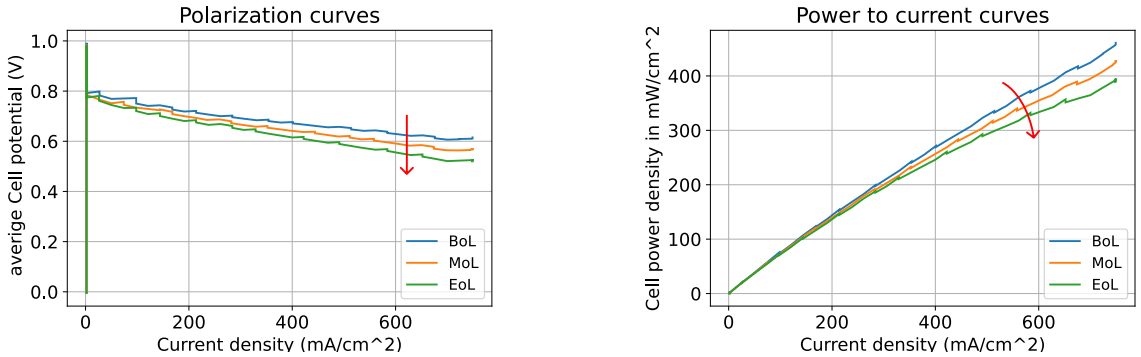

Figure 5.5: a) shows the polarization curve of the fuel cell, early, mid, and end of the test. b) shows the power to current curve, early, mid, and at the end of the test.

These figures are very comparative in shape and potential or power reduction as fuel cells tested in literature reaching EoL. The reduction of cell potential is about 15%.

6

Conclusion and recommendations

6.1. Summary

In this thesis, Nedstack cathode carbon corrosion model has been updated. The temperature is variable in both the Arrhenius equation and the kinetic governing equation but was only variable in the kinetic governing equation. This resulted in an unexpected temperature dependency on the corrosion rate. Modifying the model changed the temperature dependency to fit with PEMFC carbon corrosion theory. Now, when the temperature increases, the corrosion rate increases as well.

A goal of this research was to check if this model can be validated with the experimental data provided. With the current AST data, the model cannot be validated. In order to recognize when carbon corrosion occurs, a setup is designed that can measure the concentration of different gasses in the exhaust gas mixture of a fuel cell. During carbon corrosion, carbon material of the electrode can react with water molecules to form carbon dioxide. Nedstack acquired data, by testing a fuel cell short stack, using an accelerated stress test and a gas analyzer.

In this research the acquired data has been analyzed. The fuel cell data and gas analyzer data had a mismatch in time. The time delay, caused by the distance between the gas analyzer and the fuel cell, is found. Matching the data helps with comparing details in the gas data with occurrences in the fuel cell. A figure is made from the carbon dioxide data during one stress cycle. The values seem to change during the cycle with about 10%. These fluctuations are caused by the change in the oxygen content during the startup, constant operation, and shutdown period. Oxygen is used in the reaction with hydrogen to create power in a fuel cell. The water vapor formed during this reaction is removed via a chiller before the gas analyzer. The amount of particles entering the gas analyzer changes during the cycle, which has its implications on the carbon dioxide data. At first glance at the data, it looked like the fuel cell is producing a lot of carbon dioxide during operation if the change in oxygen concentration is not taken in to account. To get a better insight into the the carbon dioxide data these large fluctuations needed to be removed. A formula has been synthesized that removes these fluctuations in the concentrations due to the changing oxygen content. The resulting carbon dioxide data has a near-stable constant value of carbon dioxide exempt for 2 spikes. One is during startup and is a maxima, the other is a minimum and is during shutdown. The maxima I believe to be carbon corrosion. The minima can be partially explained by a stagnating flow through the cathode during shutdown. Figure 4.3c shows that stagnating flow as a spike downwards during an else constant flow of 25 nL/min. The maxima in the CO_2 data occur during startup of the fuel cell. PEMFC are prone to carbon corrosion during startup because of the forming of a hydrogen-air front at the anode. The potential of the fuel cell tends to spike during this period. The high potential makes the carbon corrosion reaction more likely to occur.

To estimate the corrosion rate during startup an equation is made that finds the extra carbon dioxide flow through the gas analyzer in mol per second. The extra carbon dioxide would be the carbon dioxide produced by the corrosion process. For that next to the compensated CO_2 date, a base level of CO_2 is determined. For the flow through the gas analyzer, necessary for the calculation, scatter is removed.

The other parameters in the equation are not data-dependent. The estimation found that 0.12 gram of carbon is lost during the whole test, which is about a fifth of the initial active carbon present at the cathode, as state by the model. If that is true the reducing effect of carbon corrosion due to the diminished carbon reserves present at the cathode should not be visible yet. This means that the area under the peak of the extra CO_2 emissions should stay about the same size for the duration of the test. The area under the peak did stay the same during the test as can be seen in table 5.1.

6.2. Conclusions and recommendations from the research

It was not possible to validate the carbon corrosion model with fuel cell and gas analyzer data from Nedstack. The model is made for a constant operation where operational temperature and cell potential are the variable parameters to find the corrosion rate. Nedstacks' AST on the other hand is built up of cyclic start-ups and shutdowns. Literature states that carbon corrosion for example is also likely to happen during, flooding and fuel starvation, when there is a hydrogen-air front during startup, dynamic load cycling, and when the fuel cell operates at open circuit voltage (OCV). At least a couple of these factors occur during the AST and are not modeled. This makes the data acquired not fit for using it to validate the model.

From the data analysis the largest CO_2 generations occurs during startup and hardly any carbon dioxide emissions are recognizable during constant operation. The model estimated that at the operational parameters of Nedstack's fuel cell the carbon of the cathode is depleted, under certain potentials and temperature settings, after 4 billion seconds (127 years). This was calculated back to the expected carbon dioxide emissions during the more constant operation part of the AST, resulting in nearly 1e-3 ppm emissions per second. This amount is insignificant compared to the fluctuation in the carbon dioxide fraction in the ambient air during the measurements.

As a change for a future setup I would suggest to implement a sensor that can measure potential both below zero and up to 2 volt. Currently, the sensor is limited between 0 and 1 Volt, which makes it is hard to interpreted the situation because we do not know how high the voltage spikes and if it becomes negative. Electrode potentials not only indicate which reactions could start to occur but also if a situation arises at a one of the electrodes, like flooding or the hydrogen-air front. Complete data can make it easier to compare with literature as well.

A reference measurement of CO_2, O_2, and N_2 in the air would be an interesting measurement to have. Now a base value for gas fractions is estimated per cycle from the data of the gas analyzer. Although believed to be accurate, a turbulent flow in the pipes and the chiller can mix the air before it enters the gas analyzer. Resulting in lower peaks and a wrong estimation of the base value of carbon dioxide.

Lastly, there is the possibility that information is lost with the removal of water by the chiller. The chiller brings a lot of advantages but there is the possibility that carbon dioxide can be buffered in liquid water. The removed water could take some carbon dioxide out of the system.

For further research, We developed the data processing procedure to calculate the accumulative sum of carbon dioxide dispersed from the exhaust of a PEMFC. It could be interesting to do an ex-situ analysis, before and after the PEMFC undergoes the AST With TEM or SEM spectroscopy, These methods can be used to measure the thickness of the carbon layer and with that the loss of carbon. This method could go a long way in validating the calculation for carbon loss following the carbon dioxide emissions.

Bibliography

[1] Nathalie Seddon et al. “Getting the message right on nature-based solutions to climate change”. In: *Global Change Biology* 27 (8 Apr. 2021), pp. 1518–1546. ISSN: 13652486. DOI: 10.1111/gcb.15513.

[2] Joeri Rogelj et al. “Paris Agreement climate proposals need a boost to keep warming well below 2 °c”. In: *Nature* 534 (7609 June 2016), pp. 631–639. ISSN: 14764687. DOI: 10.1038/nature18307.

[3] Mark Z. Jacobson et al. “100% Clean and Renewable Wind, Water, and Sunlight All-Sector Energy Roadmaps for 139 Countries of the World”. In: *Joule* 1 (1 Sept. 2017), pp. 108–121. ISSN: 25424351. DOI: 10.1016/j.joule.2017.07.005.

[4] Christian Breyer et al. “On the History and Future of 100% Renewable Energy Systems Research”. In: *IEEE Access* 10 (2022), pp. 78176–78218. ISSN: 21693536. DOI: 10.1109/ACCESS.2022.3193402.

[5] Ali Q. Al-Shetwi et al. “Grid-connected renewable energy sources: Review of the recent integration requirements and control methods”. In: *Journal of Cleaner Production* 253 (Apr. 2020). ISSN: 09596526. DOI: 10.1016/j.jclepro.2019.119831.

[6] Sheila Samsatli, Iain Staffell, and Nouri J. Samsatli. “Optimal design and operation of integrated wind-hydrogen-electricity networks for decarbonising the domestic transport sector in Great Britain”. In: *International Journal of Hydrogen Energy* 41 (1 Jan. 2016), pp. 447–475. ISSN: 03603199. DOI: 10.1016/j.ijhydene.2015.10.032.

[7] Alberto Boretti and Stefania Castelletto. “Hydrogen energy storage requirements for solar and wind energy production to account for long-term variability”. In: *Renewable Energy* 221 (Feb. 2024). ISSN: 18790682. DOI: 10.1016/j.renene.2023.119797.

[8] Omar S. Ibrahim et al. “Dedicated large-scale floating offshore wind to hydrogen: Assessing design variables in proposed typologies”. In: *Renewable and Sustainable Energy Reviews* 160 (May 2022). ISSN: 18790690. DOI: 10.1016/j.rser.2022.112310.

[9] Anusorn Kongkanand, Wenbin Gu, and Mark F. Mathias. “Proton-Exchange Membrane Fuel Cells with Low-Pt Content”. In: Springer New York, 2019, pp. 323–342. DOI: 10.1007/978-1-4939-7789-5_1022.

[10] J. A. Prithi et al. “Functionalization of carbons for Pt electrocatalyst in PEMFC”. In: *International Journal of Hydrogen Energy* 46 (34 May 2021), pp. 17871–17885. ISSN: 03603199. DOI: 10.1016/j.ijhydene.2021.02.186.

[11] “Fuel Cells”. In: (). URL: https://www.energy.gov/eere/fuelcells/fuel-cells.

[12] Fengfeng Liu et al. “An Experimental Investigation of the Effect of Platinum on the Corrosion of Cathode Carbon Support in a PEMFC”. In: *ChemSusChem* 15 (10 May 2022). ISSN: 1864564X. DOI: 10.1002/cssc.202102726.

[13] K. C. Neyerlin et al. “Cathode Catalyst Utilization for the ORR in a PEMFC”. In: *Journal of The Electrochemical Society* 154 (2 2007), B279. ISSN: 00134651. DOI: 10.1149/1.2400626.

[14] D. A. Noren and M. A. Hoffman. “Clarifying the Butler-Volmer equation and related approximations for calculating activation losses in solid oxide fuel cell models”. In: *Journal of Power Sources* 152 (1-2 Dec. 2005), pp. 175–181. ISSN: 03787753. DOI: 10.1016/j.jpowsour.2005.03.174.

[15] Colleen Spiegel. “Polarization Curves”. In: (May 2022). URL: https://www.fuelcellstore.com/blog-section/polarization-curves.

[16] Abdulrazzak Akroot, Özgür Ekici, and Murat Köksal. “Process modeling of an automotive pem fuel cell system”. In: *International Journal of Green Energy* 16 (10 Aug. 2019), pp. 778–788. ISSN: 15435083. DOI: 10.1080/15435075.2019.1641105.

[17] Zhongxin Song et al. “Atomic layer deposited tantalum oxide to anchor Pt/C for a highly stable catalyst in PEMFCs”. In: *Journal of Materials Chemistry A* 5 (20 2017), pp. 9760–9767. ISSN: 20507496. DOI: 10.1039/c7ta01926b.

[18] Marine Jouin et al. *Estimating the end-of-life of PEM fuel cells: Guidelines and metrics*. 2016. URL: https://hal.science/hal-02380401.

[19] Mohamed Louzazni, Sameer Al-Dahidi, and Marco Mussetta. “Fuel cell characteristic curve approximation using the Bezier curve technique”. In: *Sustainability (Switzerland)* 12 (19 Oct. 2020). ISSN: 20711050. DOI: 10.3390/su12198127.

[20] Haojie Wang et al. “Cathode Design for Proton Exchange Membrane Fuel Cells in Automotive Applications”. In: *Automotive Innovation* 4 (2 May 2021), pp. 144–164. ISSN: 25228765. DOI: 10.1007/s42154-021-00148-y.

[21] Y. Shao-Horn et al. “Instability of supported platinum nanoparticles in low-temperature fuel cells”. In: *Topics in Catalysis* 46 (3-4 Dec. 2007), pp. 285–305. ISSN: 10225528. DOI: 10.1007/s11244-007-9000-0.

[22] Junjie Zhao, Zhengkai Tu, and Siew Hwa Chan. *Carbon corrosion mechanism and mitigation strategies in a proton exchange membrane fuel cell (PEMFC): A review*. Mar. 2021. DOI: 10.1016/j.jpowsour.2020.229434.

[23] S. Maass et al. “Carbon support oxidation in PEM fuel cell cathodes”. In: *Journal of Power Sources* 176 (2 Feb. 2008), pp. 444–451. ISSN: 03787753. DOI: 10.1016/j.jpowsour.2007.08.053.

[24] Felix N. Büchi, Thomas J. Schmidt, and Minoru Inaba. *Polymer electrolyte fuel cell durability*. Springer New York, 2009, pp. 1–507. ISBN: 9780387855349. DOI: 10.1007/978-0-387-85536-3.

[25] Carl A. Reiser et al. “A reverse-current decay mechanism for fuel cells”. In: *Electrochemical and Solid-State Letters* 8 (6 2005). ISSN: 10990062. DOI: 10.1149/1.1896466.

[26] Yunqi Li et al. “Analytical modeling framework for performance degradation of PEM fuel cells during startup-shutdown cycles”. In: *RSC Advances* 10 (4 2020), pp. 2216–2226. ISSN: 20462069. DOI: 10.1039/c9ra09572a.

[27] Viraisha Bhoewar et al. *Characterisation and modelling of carbon support corrosion in PEM fuel cells*. 2023.

[28] Leslie Eudy and Matthew Post. *Fuel Cell Buses in U.S. Transit Fleets: Current Status 2017*. 2017. URL: www.nrel.gov/publications..

[29] J. Stumper A. P. Young and E. Gyenge. “Characterizing the Structural Degradation in a PEMFC Cathode Catalyst Layer: Carbon Corrosion”. In: *J. Electrochem. Soc* 156 (B913 2009). ISSN: 10990062. DOI: 10.1149/1.3139963.

[30] Bolahaga Randrianarizafy et al. “Modelling carbon Corrosion during a PEMFC startup: Simulation of mitigation strategies”. In: *Energies* 13 (9 May 2020). ISSN: 19961073. DOI: 10.3390/en13092338.

[31] Hendrik Schulenburg et al. “3D Imaging of catalyst support corrosion in polymer electrolyte fuel cells”. In: *Journal of Physical Chemistry C* 115 (29 July 2011), pp. 14236–14243. ISSN: 19327447. DOI: 10.1021/jp203016u.